Available online at www.sciencedirect.com
SCIENCE DIRECT®
Polymer 45 (2004) 3063–3071
polymer
www.elsevier.com/locate/polymer

Microstructures and mechanical properties of polypropylene/polyamide 6/polyethelene-octene elastomer blends

Shu-Lin Bai[a,*], Gong-Tao Wang[a], Jean-Marie Hiver[b], Christian G'Sell[b]

[a]*Department of Mechanics and Engineering Science, Peking University, 100871 Beijing, China*
[b]*Laboratoire de Physique des Matériaux, Ecole des Mines de Nancy, Parc de Saurupt, 54042 Nancy Cedex, France*

Received 24 September 2002; received in revised form 21 January 2004; accepted 11 February 2004

Abstract

A series of polymer blends were designed and manufactured. They are composed of three phases: polypropylene (PP), polyamide-6 (PA6) and polyethylene-octene elastomer (POE) grafted with maleic anhydride. The weight fraction of PA6 was adjusted from 0 to 40% by increments of 10%, and the weight fraction of POE was systematically half that of PA6. The morphology, essentially made of PA6 particles dispersed in the PP matrix, was characterised by scanning electron microscopy (SEM) and transmission electron microscopy (TEM). In the extruded plates prepared with the blends, the shape of the dispersed PA6 particles showed an elongated ellipsoidal shape, whose aspect ratio increased somehow with alloying content. The POE modifier was observed both as a thin interlayer (less than 100 nm thickness) at the PP/PA6 interface, and as a few isolated particles. The elastic modulus and yield stress in tension are nearly constant for PP and blends. By contrast, the notched Izod impact strength increases very much with alloying content. This remarkable effect is interpreted in terms of POE interphase cavitation, enhanced plastic shear deformation and resistance of PA6 particles to crack propagation.

Keywords: PP/PA6/POE blends; Microstructure; Mechanical properties

1. Introduction

Polypropylene (PP) is a low-cost polymer with versatile applications but with limited impact strength. Polyamides (PA) find also wide engineering applications due to their easy processing, low friction, wear resistance, and high melting temperature, but they are limited by their higher cost, critical brittleness under triaxial loading and considerable water uptake. In the past decades, the blends of PP and PA were studied in much detail. An advantage of this system is that reactive schemes are similar for both polymers [1]. In order to favour better compatibility between PP and PA phases and consequently better properties, the blends are usually prepared with rubber-like modifiers [2–9]. The elastomers mostly utilized are the maleated ethylene-propylene random copolymer (EPR), the maleated ethylene-propylene-diene monomer (EPDM) and the maleated styrene-ethylene-butylene-styrene block copolymer (SEBS) [10–13]. These functionalised polymers copolymerise in situ by grafts with PA, giving rise to strong links between the two phases.

The morphology of PP/PA blends, added with a rubber modifier, was thoroughly studied by Gonzalez-Montiel et al. [14,15] (PP/PA6/EPR and PP/PA6/SEBS systems), Wong et Mai [16] (PP/PA66/SEBS) and Rosch et al. [17,18] (PP/PA6/SEBS). By increasing the PA/PP ratio, the above authors showed that the morphology of the blends changed from PA particles dispersed in a PP matrix to PP particles in a PA matrix. Inversion occurs near to the 50/50 composition. As for the modifier, it migrates in the melt towards the PA/PP interface, thus giving rise to 'core-shell' particles with a rigid core (PP or PA according to composition) encapsulated in a rubber shell. In many cases, significant amount of the modifier was observed in isolated rubber particles dispersed in the matrix.

In the blends based on the PP/PA system, microscopic cavitation and macroscopic volume dilatation under tensile deformation were investigated with much attention by different authors. For PA6/PP/EPR blends, Gonzalez-Montiel et al. [19] found that cavitation is activated, for a

* Corresponding author. Tel.: +86-10-62753328; fax: +86-10-63751444.
E-mail address: slbai@pku.edu.cn (S.L. Bai).

0032-3861/$ - see front matter © 2004 Published by Elsevier Ltd.
doi:10.1016/j.polymer.2004.02.070

wide range of strain rates, in the rubber interlayer between PA6 and PP particles and in the dispersed rubber particles as well. Unlikely, for the PA6/PP/SEBS blends, volume change is recorded only at high strain rates. Furthermore, in PA66/PP/SEBS blends, Wong and Mai [20] observed that the cavitation in the rubber interlayer relieves the hydrostatic tension in the matrix and consequently favours shear yielding around the core-shell particles. This effect is important, because it hinders crack propagation in the material by promoting plastic dissipation at crack tips.

However, in most blends, the improvement of material toughness is accompanied by a marked decrease of the tensile modulus, E, and/or the yield stress, σ_y, which limits seriously the applicability of these materials. This is the reason why we undertook a systematic work in order to understand the microstructural interrelations between elastic, plastic and cavitation processes in selected blends. In a preliminary work [21], we found that polyethylene-octene elastomer (POE) grafted with maleic anhydride was more efficient than the previously utilized modifiers for the PP/PA6 system, since it provides a high impact strength.

The aim of this paper is to study in more detail a series of PP/PA6/POE blends whose potential interest was rarely reported before. Here we focus our attention on the influence of composition on morphology and standard mechanical properties (engineering stress–strain curves in tension and Izod impact strength). Further investigation on the interaction between cavitation and shear yielding mechanisms, characterized by in situ volume strain measurement and microscopic observation, will be presented in the papers to be published later.

2. Experimental

2.1. Materials

The compositions of the PP/PA6/POE blends under investigation are listed in Table 1. The total alloying (PA6 + POE) varies from 0 wt% (noted PP for short) to 60 wt% (noted BD16). In all materials, the percentage of PA6 is twice larger than the percentage of POE-g-MA.

The polypropylene (PP) was obtained from Liaoyang Petrochemical Corp., Peoples Republic of China (ref. 401), and the polyamide 6 (PA6) from Shanghai Plastics Production Factory No. 18, Peoples Republic of China. The polyethylene-octene modifier (POE), obtained from Dow Chemical Co. (octene content of 9.5% and melt flow index of 3.5 g/10 min), was grafted in the laboratory with maleic anhydride at a ratio of about 1% in weight.

Table 1
Composition of the blends studied

Blend	PP (wt%)	PA6 (wt%)	POE-g-MA (wt%)	Total alloying (wt%)
PP	100	0	0	0
BD13	85	10	5	15
BD14	70	20	10	30
BD15	55	30	15	45
BD16	40	40	20	60

All materials were dry blended together in a high-speed blender following the pre-designed composition ratios. Then a co-rotating twin-screw extruder (SHJ-30, diameter 30 mm) was employed at a screw speed of 110 rpm and barrel temperatures of 190–200–210–200 °C. The pelletised blends were dried and injection moulded into standard ASTM specimens in an injection-moulding machine (SZ-160/80 NB) for mechanical tests.

2.2. Mechanical testing

The tensile tests were carried out on a universal testing machine (CSS-2210) under ambient condition at a nominal strain rate of $5.55 \times 10^{-4}\,s^{-1}$. The tensile specimen dimensions meet the requirement of ASTM D638M standard. Average of at least three tests for each blend is reported.

The notched Izod impact strength of the materials was measured with an impact-testing machine (CSI-137C) according to National Standard Testing Methods GB1843-80. All specimens have a dimension of 63 mm × 12.70 mm × 12.70 mm. For each kind of blends, six specimens were tested and the average value is given.

The dynamic mechanical thermal analysis (DMTA) was carried out under bending by using DMTA MKIII (Polymer Laboratories) at a frequency of 1 Hz, with the sample dimension of 45 mm × 9 mm × 2.10 mm. The heating rate was 2 °C/min.

2.3. Morphological observation

The morphological study includes the intrinsic microstructures of the blends and the morphological characteristics of the fractured surfaces after impact tests. For the first objective, the cryo-fractured surfaces were prepared and then observed with an Amary-1910FE scanning electron microscope (SEM). In order to characterize the different phases present in the blends, one series of cryo-fractured surfaces was etched with formic acid for 24 h to remove the PA6 phase. The surface was then coated with gold. The size distribution of the PA6 phase in blends was determined by measurements of approximately 300 domains from sets of cryo-fractured SEM micrographs. The observation of fractured surfaces by impact tests was carried out with the same SEM. Fig. 1 shows the method to cut the tensile samples in view of obtaining cross-sections and longitudinal sections for SEM observation.

Moreover, a Hitachi H-800 transmission electron microscope (TEM) was also used to reveal the details of dispersed phases and the interface. Ultra-thin sections having minimum thickness of 60 nm were cut using a LKB Ultratome V ultramicrotome under the condition of sample

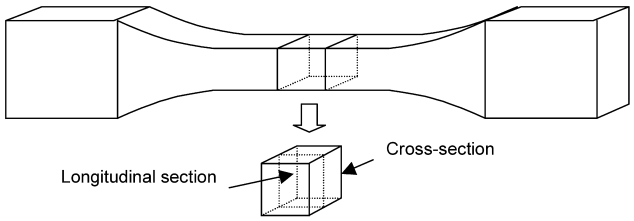

Fig. 1. Method to cut sections for SEM observation.

temperature −80 °C and knife temperature −70 °C. The sections were stained, respectively, with RuO_4 vapour for 20 min and OsO_4 for 40 min in order to enhance contrast.

3. Experimental results

3.1. Morphological characterization

In Fig. 2 are shown the SEM micrographs of cryo-fractured cross-sections etched with formic acid of the four blends. The large quantity of pits (or holes) observed correspond to PA6 particles removed by the formic acid etching. Since formic acid does not react with POE, and hence the PA6 particles coated with POE should not be removed, the observed pits are presumably of three types: (i) PA6 particles not coated with POE. (ii) PA6 particles partially coated with POE and, (iii) PA6 particles with debonded PA6/POE interface. It is known that the succinic anhydride group of the maleic anhydride grafted POE is able to react with PA6 amine terminal groups to form POE-*co*-PA6 copolymer that strongly tends to concentrate at the PP/PA6 interfaces during melt processing.

The histograms in Fig. 3 gives the approximately normal distribution of PA6 particle diameters and the graph in Fig. 4 shows the influence of total alloying on the 'peak diameter' (most probable diameter in the distributions). The most striking feature is that the particles with highest peak diameter were found in the blend with 15% alloying (BD13), while particles are 70% finer in the blends with higher alloying contents. Also, it is seen that the diameter distribution is narrower in the blends at 15 and 30% alloying contents and wider in the other two blends. Subsequently, the blend BD14 (20% PA6 + 10% POE) combines the finest PA6 particles (peak diameter about 0.4 μm) and the narrowest size distribution (diameter within the range from 0.1 to 1.1 μm).

The SEM micrographs in Fig. 5 show the morphology of longitudinal sections of the blends and subsequently etched with formic acid. Since the exposed surface is parallel to the flow direction of the injection-moulded samples, the micrographs are likely to reveal some process-induced orientation in the morphology. Actually, one notes in Fig. 5 that many particles exhibit ellipsoidal shapes, whose major axis is parallel to the injection direction. The aspect ratio of the ellipsoids is variable from a specimen to another. While most particles are quasi-spherical in blends BD13 and BD14, they are markedly elongated in BD15 and BD16.

The series of TEM micrographs in Fig. 6 shows longitudinal sections stained with RuO_4, at medium magnification. As stated before, RuO_4 stains all phases in the blend but with different colours. The light greyish and

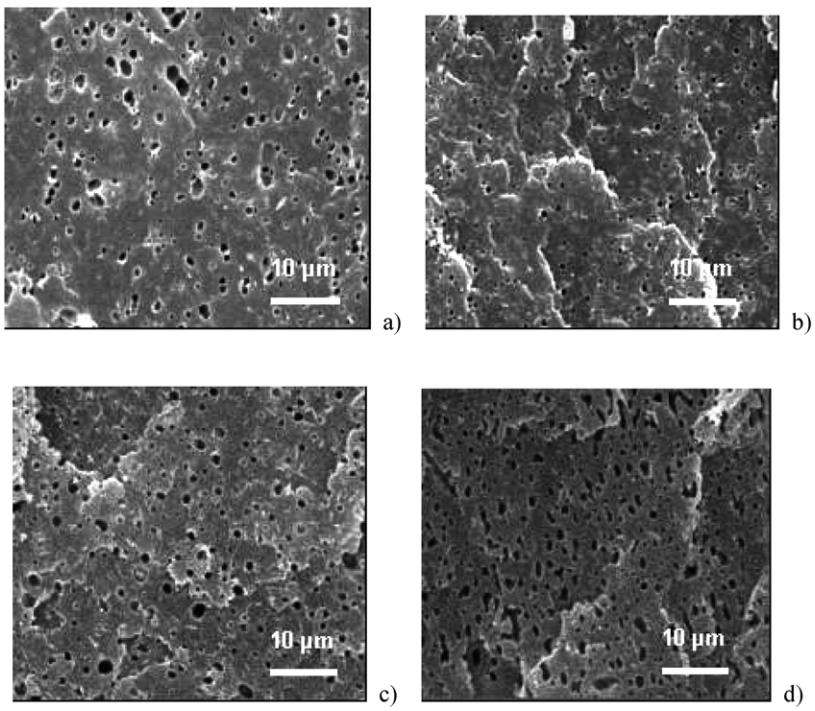

Fig. 2. Cross-sections etched with formic acid. (a) BD13, (b) BD14, (c) BD15, (d) BD16 (all black pits are left by PA6 particles).

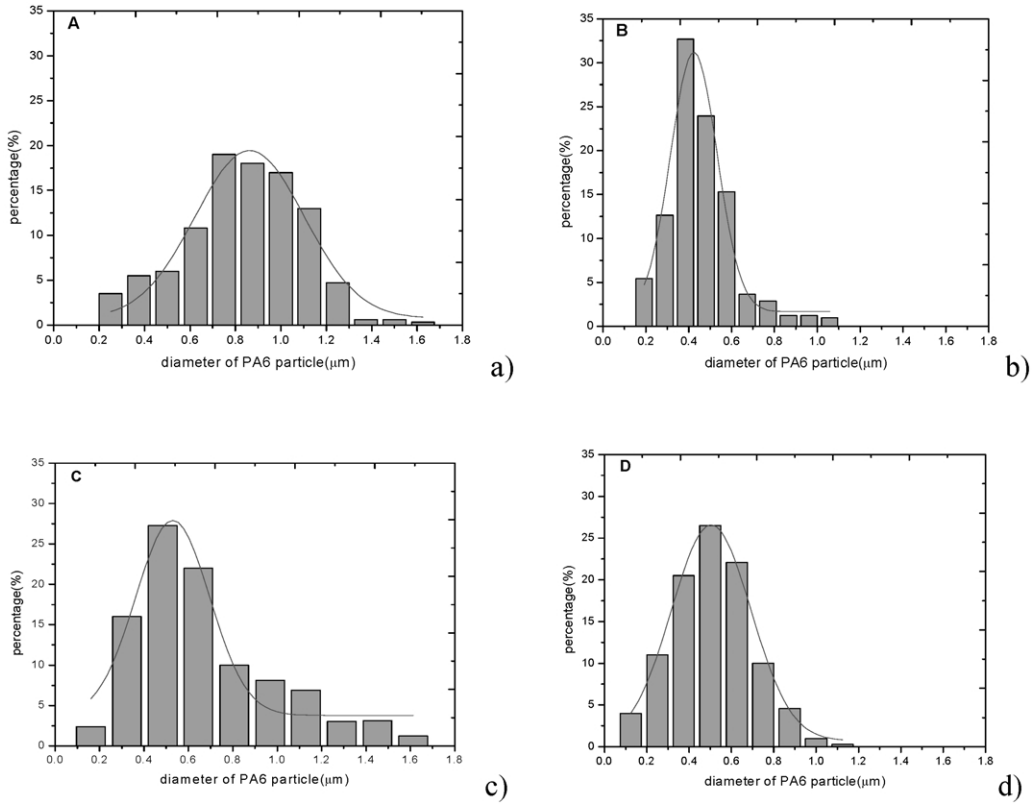

Fig. 3. PA6 particle size distribution. (a) BD13, (b) BD14, (c) BD15, (d) BD16.

continuous phase is the PP matrix. As for the large black ellipsoids, they correspond to PA6 particles. The TEM observation confirms that their aspect ratio depends on the alloy content: the most regular spheres are observed in BD14, and the most elongated ellipsoids in BD15 and BD16. The magnification of the TEM micrographs being 10 times larger than that of the SEM images of Fig. 5, finer particles are now distinguishable with a size smaller to 0.2 μm. A few ones are black and correspond to the lower wing of the size histogram of PA6 particles. Other ones, more greyish, are identified as isolated POE particles. The

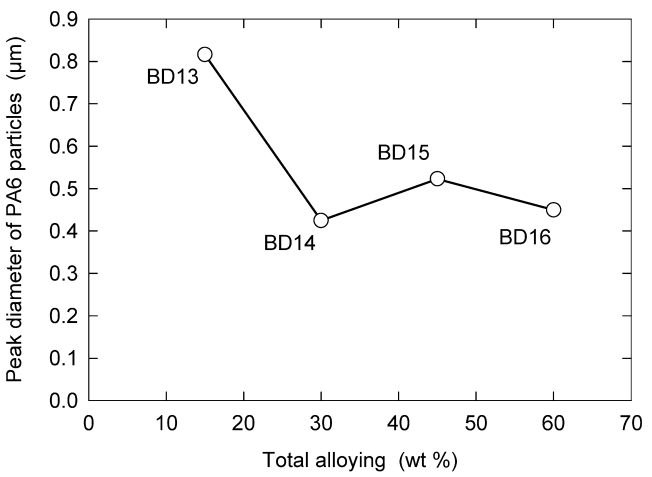

Fig. 4. Mean diameter of PA6 particles versus total alloying.

above investigation confirms that the BD14 shows the most regular particle morphology, in terms of size, distribution and isotropy, among the blends of the PP/PA6/POE series. Another feature revealed by the TEM micrographs is the presence of bright inclusions in the interior of the large PA6 particles in the BD15 and BD16 blends. Owing to their similar contrast with the PP matrix, these species are considered to be PP particles trapped within the PA6 like in 'salami' morphology. If the PA6 content were increased furthermore, the morphology should become a continuous PA6 matrix with embedded PP particles. The big and irregular PA6 'patches' in BD16 announces this transition, but in this blend, the PP phase is still continuous.

The TEM micrographs in Fig. 7 were obtained at higher magnification. Here the staining agent is OsO_4; since it cannot react with PP and PA6, only POE phases are stained in dark. The POE interlayer around the PA6 particles appears as a thin and black circle. The thickness of POE interlayer increases from 10 to 100 nm as alloying content is increased.

3.2. Dynamic mechanical thermal analysis

The curves in Fig. 8(a) and (b), obtained by dynamic mechanical thermal analysis, show the variation of storage modulus and loss tangent for PP and for the blends as a function of temperature. It is noted that blending PP with PA6 and POE has small but significant influence on

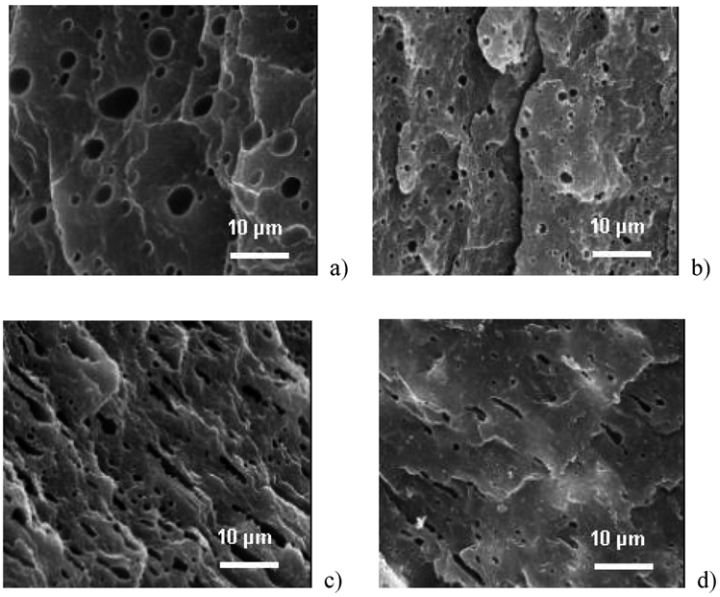

Fig. 5. Longitudinal section etched with formic acid. (a) BD13, (b) BD14, (c) BD15, (d) BD16.

viscoelastic properties. The storage modulus decreases with the alloying content, while the loss tangent increases. Two distinct transition temperatures are recorded for PP, one at about 18 °C that corresponds to the β-transition, and the other at about 80 °C representing the α-relaxation. Most blends have two peaks just as PP (with greater tan δ owing to the presence of POE), except for BD16 that does not show any β-transition. This phenomenon is possibly related to the balanced concentration in PA6 and PP. Since PA6 has a higher transition temperature than PP (about 60 °C), the concurrence between PA6 and PP is responsible for the disappearance of PP peak at β-transition for BD16 that has equal content of PP and PA6. Additionally, the blends show a low temperature peak at −50 °C, which corresponds to the glass transition of POE.

3.3. Mechanical properties under tension

Fig. 9 shows nominal stress–strain curves of PP and blends under uniaxial tension at room temperature. It is seen that neat PP has the highest yield stress, about 32 MPa, followed by a sharp load drop (necking process) and a rather brittle fracture at a nominal strain not larger than 17%. Unlikely, for the most blended material, BD16, no yield drop is observed. Tensile stress progressively saturates at strains over 10%, and ultimate behaviour shows neither softening nor hardening up to the maximum strain applied. The tensile behaviour of other blends shows a limited yield drop followed by a stress plateau. The above evolution describes the brittle-to-ductile transition between PP and the blends. The consumed energy during the deformation,

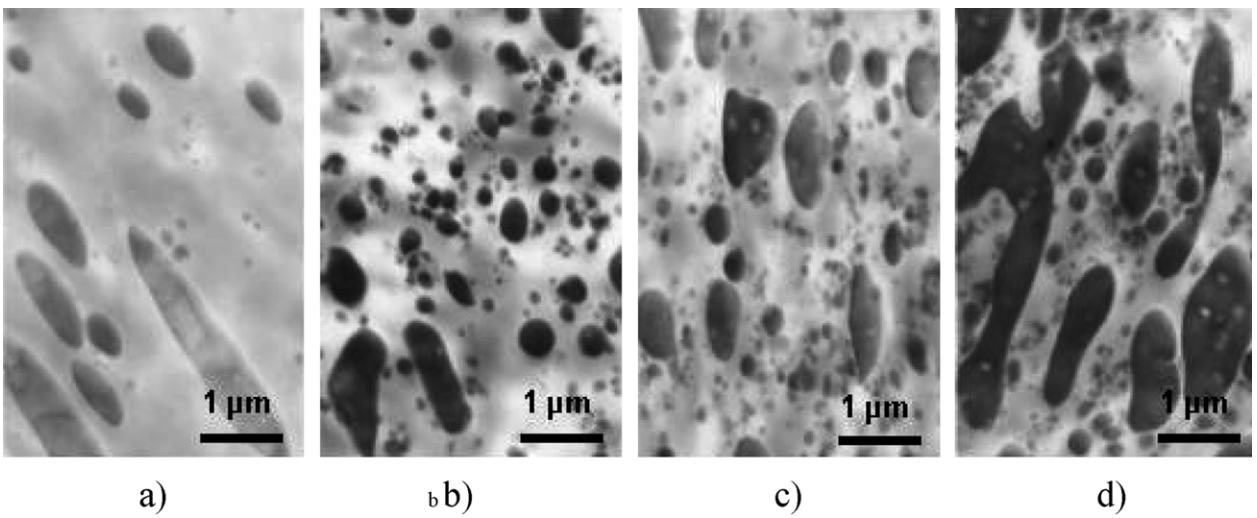

Fig. 6. TEM micrographs of the sections stained with RuO_4 (a) BD13, (b) BD14, (c) BD15, (d) BD16.

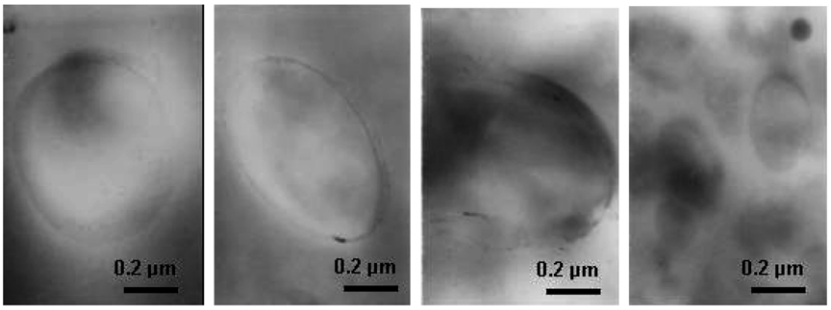

Fig. 7. TEM micrographs of the sections stained with OsO_4 (a) BD13, (b) BD14, (c) BD15, (d) BD16.

represented by the area below the stress–strain curve, increases continuously with increasing alloying content.

The mechanical properties of the blends are characterised by the Young's modulus, E, and the yield stress, σ_y. Fig. 10 shows that E exhibits a moderate (almost linear) decrease with the alloying content. Since PA6 is intrinsically more rigid than PP, this evolution should be attributed to the presence of the POE elastomer whose flexibilising effect appears to override the stiffening effect of PA6. Similarly, Fig. 11 shows that σ_y is weakly dependent on alloying content. It decreases only by about 12.5% from PP to BD14 blend and then increases slightly for the blends with higher alloying content.

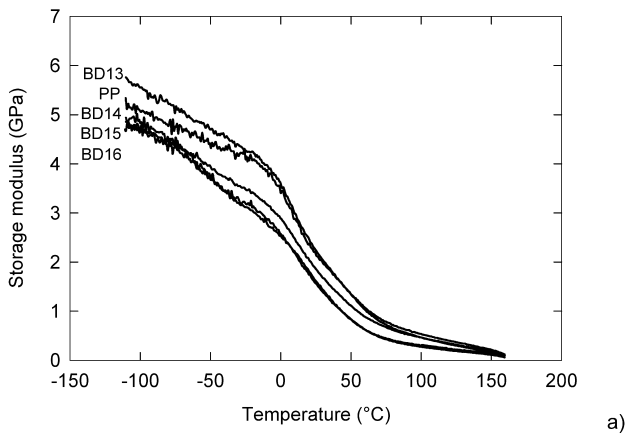

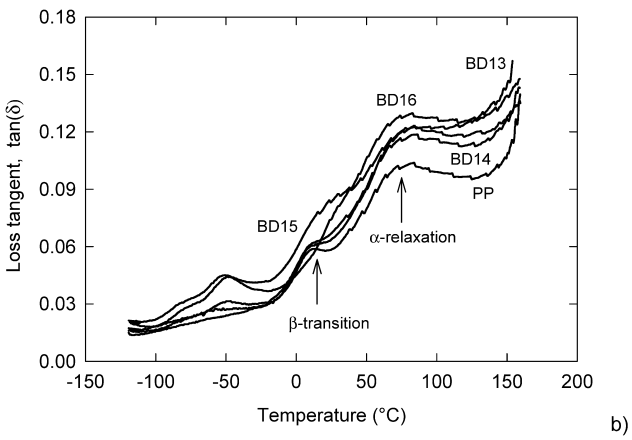

Fig. 8. (a) Storage modulus, E', of PP and blends versus temperature (b) loss tangent, tan δ, of PP and blends versus temperature.

3.4. Toughness by impact loading

The most interesting property of the PP/PA6/POE blends is their improved resistance to impact. The graph in Fig. 11 gives the notched Izod impact strength as a function of alloying content. It is seen that the impact strength of the blends increases considerably with PA6/POE content, reaching a value of 158 J/m for the BD16 blend, that is 4.7 times greater than that of PP. These data contrast with the results obtained previously [21], which showed that: (i) the simple addition of PA6 to PP merely results in a small increase of impact strength and, (ii) the use of PP-g-MA as a compatibiliser causes a decrease of the impact strength. Therefore, the large toughening observed in the systems investigated in this work is certainly related to the effect of the POE compatibiliser.

SEM micrographs of impact-fractured surfaces of blends are shown in Fig. 12. The spherical particles are mainly PA6 and the black pits correspond to sites where PA6 particles were extracted from the PP matrix. Less and less PA6 particles are observed on the fracture surface as the PA6 content increase. The interlayer thickness is rather small when the POE content is as low as 5–10%, so that failure

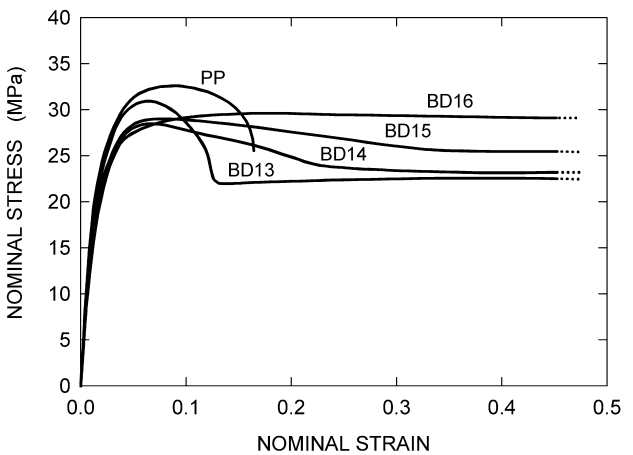

Fig. 9. Tensile stress–strain curves of PP and blends.

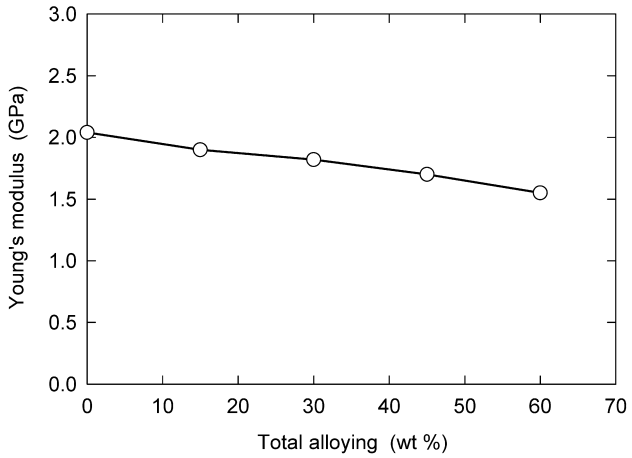

Fig. 10. Young's modulus versus alloying content.

occurred probably at the PA6/POE interface, in such a way that the PA6 surface is exposed. When the POE content increases, the interlayer becomes thicker and the failure occurs consequently at the PP/POE interface. This means that PA6 particles remain covered by POE after failure.

4. Discussion

The Young's modulus of the blends depends on the volume fraction their constituents, the rigidity of the phases, and the aspect ratio of the dispersed particles. Numerous publications are found on the theoretical prediction of E for particle-filled composites. The theoretical models are basically established from the Eshelby's equivalent inclusion method, which was developed extensively elsewhere [22–24]. It is well known [25] that adding rigid particles such as glass beads into a polymer matrix is likely to increase E, while soft particles reduce this property. In our case, two phases are simultaneously incorporated in PP: rigid PA6 and rubber-like POE. The moduli of PA6 and POE are slightly greater and moderately smaller than that of PP, respectively. Therefore, they have opposite influences on the modulus of the blends. The morphology of the blends

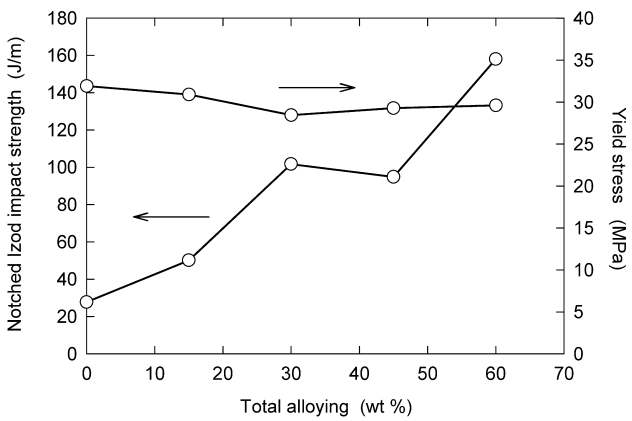

Fig. 11. Notched Izod impact strength and yielding of PP and blends.

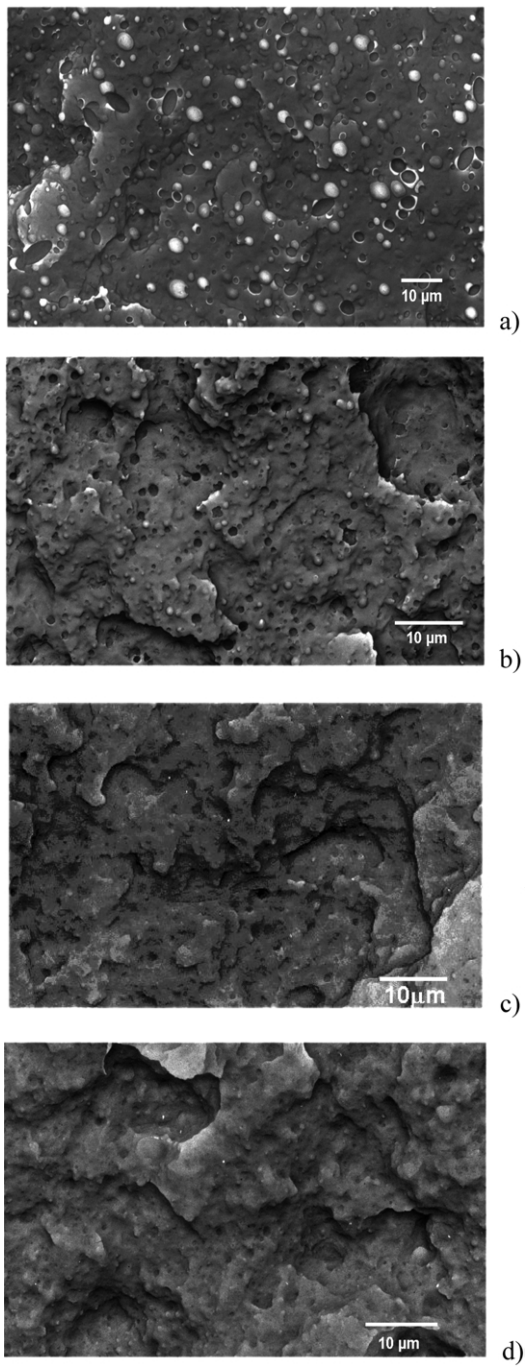

Fig. 12. Micrographs of impact-fractured surfaces of blends (a) BD13, (b) BD14, (c) BD15, (d) BD16.

studied is rather complex, with several kinds of phases: (i) spherical or ellipsoidal PA6 particles with small PP particles embedded in some of the biggest ones and, (ii) POE interlayers and particle. Furthermore, the ellipsoidal shape of the PA6 particles in BD15 and BD16 is likely to increase E in the direction of orientation, in a similar way as in composites reinforced with oriented fibres. The theoretical modelling of elastic modulus for the PP/PA6/POE blends is ahead of the scope of this publication. It will be fulfilled in the future.

Concerning σ_y, the combined influence of PA6 and POE can change greatly the behaviour of PP. Grossly, it could be envisaged that PA6 and POE particles have opposite effects on σ_y, similarly to their effects on E. However, yield stress is also controlled by the characteristics of particles (volume fraction, average diameter, size distribution, interfacial adhesion, etc.). The strong adhesion at the interface, promoted by the thin rubber interlayer of the small particles, favours an increase of tensile strength [26,27]. Conversely, increasing particle size and interlayer thickness cause premature interfacial debonding and decrease yield stress.

The cavitation of isolated rubber particles and rubber interlayers represents the main mechanisms of damage and volume dilatation for polymer blends. Since cavitation in PA6 particles was not encountered in this work neither by other authors, deformation damage is essentially controlled by rubber cavitation and interfacial debonding. The cavitation of rubber particles was observed by us in TEM micrographs and will be presented, together with the volume dilatation, in our next publication. As for the interfacial debonding, it was shown previously under tension in SEM micrographs [28].

On the basis of the experimental facts reported above, it is now possible to describe, at least schematically, the essential toughening mechanisms of the PP/PA6/POE blends. The dissipation of impact energy in the blends is probably due to following factors: (i) the isolated elastomer particles play a small but significant role in either arresting the cracks or at least reducing their propagation rate, (ii) the high adhesion of the interfacial layer avoids early decohesion at the POE interphase between the PP matrix and the PA6 particles, and is later capable of cavitation, (iii) the ellipsoidal geometry of the particles improves somehow the impact resistance thanks to its favourable orientation perpendicular to the crack propagation direction. Fig. 13 gives a schematic representation of toughening mechanisms in the blends. For blends with low alloying content, such as BD13 and BD14, the POE interlayer is very thin and PA6 particles are mostly spherical. The crack propagates easily across the section and leaves a smooth fracture surface as shown by the micrographs in Fig. 12(a) and (b). By contrast, for blends with high alloying content, such as BD15 and BD16, the POE interlayer is thick and PA6 particles are highly elongated, which result in a rough fracture surfaces as shown by Fig. 12(c) and (d).

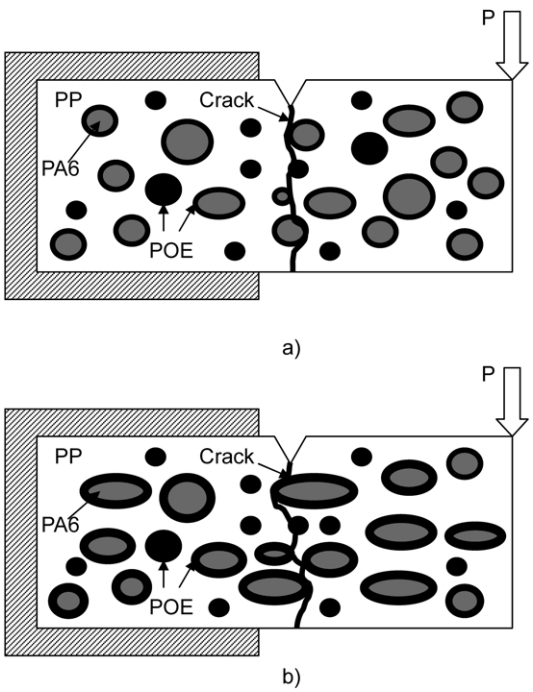

Fig. 13. Failure mechanisms under impact loading of the blends low alloying content with thin POE interlayer high alloying content with thick POE interlayer.

5. Conclusions

This work, devoted to the morphology and properties of ternary PP/PA6/POE polymer blends is based on microscopic observation (SEM and TEM) and on the determination of mechanical properties under tension and impact. In these blends, the rubber modifier is grafted with maleic anhydride to promote adhesion.

The SEM micrographs show that PA6 forms particles, the size of which obeys a normal distribution. The blend with 20 wt% PA6 + 10 wt% POE shows the best dispersion of PA6 particles. The TEM micrographs reveal the existence of a POE interlayer around the PA6 particles (thickness below 100 nm) and independent POE particles dispersed in the PP matrix. When POE + PA6 content is high, the spherical PA6 particles tend to become irregular ellipsoids oriented along the injection direction.

It was found that the toughness of the PP/PA6/POE blends increases with alloying content, the material with 40 wt% PA6 and 20 wt% of POE exhibiting a notched Izod impact strength 4.7 times higher than that of neat PP. Furthermore, this improvement was gained without important decrease of Young's modulus or yield stress.

A qualitative micromechanical model taking into account the complex morphology was presented, that explains these valuable properties. The high toughness is controlled by the intrinsic resistance of the PA6 particles, and by the profuse cavitation in the POE isolated particles and interlayers. As for the good modulus and yield strength, it is due to the adequately combined effect of rigid PA6 and flexible POE, the orientation of the ellipsoidal PA6 particles playing positive role in this balance.

Acknowledgements

This work is supported by the National Natural Science Foundation of China under grant of 10272005 and

10032010, by the Excellent Young Teachers Program of MOE, Peoples Republic of China and also by the cooperation programme PRA between China and France. The authors also thanks the School of Mines (INPL, Nancy) for providing a visiting professor fellowship to one of us (S.L. Bai).

References

[1] Lohse DJ, Datta S. Soc Plast Engng, ANTEC 1992;38:1036–8.
[2] Lu M, Keskkula H, Paul DR. Polymer 1993;34:1874–85.
[3] Willis JM, Favis BD. Polym Engng Sci 1988;28:1416–26.
[4] Jo WH, Kim HG, Chae SH. Polym J 1993;25:1023–31.
[5] Oshinski A, Keskkula H, Paul DR. Polymer 1992;33:284–93.
[6] Hobbs SY, Bopp RC, Watkins VH. Polym Engng Sci 1983;23:380–9.
[7] Merle G, Yong-Sok O, Pillot C, Sautereau H. Polym Testing 1985;5: 37–43.
[8] Wu S. Polymer 1985;26:1855–63.
[9] Wu S. J Appl Polym Sci 1988;35:549–61.
[10] Borggreve RJM, Gaymans RJ, Schuijer J, Ingen-Housz JF. Polymer 1987;28:1489–96.
[11] Borggreve RJM, Gaymans RJ. Polymer 1989;30:63–70.
[12] Oshinski A, Keskkula H, Paul DR. Polymer 1992;33:268–83.
[13] Cimmino S, Coppola F, D'Orazio L. Polymer 1986;27:1874–84.
[14] Gonzales-Montiel A, Keskkula H, Paul DR. Polymer 1995;36: 4587–603.
[15] Gonzales-Montiel A, Keskkula H, Paul DR. Polymer 1995;36: 4605–20.
[16] Wong SC, Mai YW. Polymer 1999;40:1553–66.
[17] Rosch J, Mulhaupt R. Polym Bull 1994;32:697–704.
[18] Rosch J. Polym Engng Sci 1995;35:1917–22.
[19] Gonzales-Montiel A, Keskkula H, Paul DR. Polymer 1995;36: 4621–37.
[20] Wong SC, Mai YW. Polymer 2000;41:5471–83.
[21] Zeng N, Bai SL, G'Sell C, Mai YW. Polym Int 2002;51:1439–47.
[22] Ma HL, Hu GK, Huang ZP. Mech Mater 2004;36:359–68.
[23] Hu GL, Weng GJ. Acta Mech 2000;140:31–40.
[24] Sarvestani, Alireza S. Int J Solids Struct 2003;40:7553–66.
[25] Bai SL, Cao K, Chen JK, Liu ZD. Polym Polym Compos 2000;8: 413–8.
[26] Bai SL, Chen JK, Huang ZP, Yu ZZ. J Mater Sci Lett 2000;19: 1587–9.
[27] Bai SL, Chen JK, Huang ZP, Liu ZD. Polym Int 2001;50:222–8.
[28] Bai SL, Wang M. Polymer 2003;44:6637–47.